IJNAOE
©SNAK, 2015

Int. J. Nav. Archit. Ocean Eng. (2015) 7:364~374
http://dx.doi.org/10.1515/ijnaoe-2015-0025
pISSN: 2092-6782, eISSN: 2092-6790

Study on variation in ship's forward speed under regular waves depending on rudder controller

Sung-Soo Kim[1], Soon-Dong Kim[2], Donghoon Kang[3], JongHyun Lee[3],
Seung Jae Lee[4] and Kwang Hyo Jung[5]

[1]*Department of Ocean System Engineering, Gyeongsang National University, Korea*
[2]*Daewoo Shipbuilding & Marine Engineering Co., Ltd., Korea*
[3]*Department of Naval Architecture and Ocean Engineering &*
The institute of Marine Industry, Gyeongsang National University, Korea
[4]*Division of Naval Architecture and Ocean Systems Engineering, Korea Maritime and Ocean University, Korea*
[5]*Department of Naval Architecture and Ocean Engineering, Pusan National University, Korea*

ABSTRACT: *The purpose of this research is to compare and analyze the advanced speed of ships with different rudder controller in wavy condition by using a simulation. The commercial simulation tool named AQWA is used to develop the simulation of ship which has 3 degree of freedom. The nonlinear hydrodynamic force acting on hull, the propeller thrust and the rudder force are calculated by the additional subroutine which interlock with the commercial simulation tool, and the regular wave is used as the source of the external force for the simulation. Rudder rotational velocity and auto-pilot coefficients vary to make the different rudder controller. An advanced speed of ships depending on the rudder controller is analyzed after the autopilot simulations.*

KEY WORDS: Rudder controller; Rudder rotational velocity; Advance speed of ship; Regular wave; Autopilot.

NOMENCLATURE

A_R	Rudder area	$F_{W,i}$	Wave forces, i=1(Surge), i=2(Sway), i=6(Yaw)
B	Ship breadth	g	Gravity
C_b	Block coefficient	$K(t)$	Stability coefficient matrix
C	Linear damping matrix	K_D	Differential coefficient for autopilot
D_p	Propeller diameter	K_P	Proportional coefficient for autopilot
d_m	Ship draft	K_I	Integral coefficient for autopilot
$F_{H,i}$	Hull forces, i=1(Surge), i=2(Sway), i=6(Yaw)	L	Ship length
$F_{P,i}$	Propeller forces, i=1(Surge)	M_s	Ship mass matrix
$F_{R,i}$	Rudder forces, i=1(Surge), i=2(Sway), i=6(Yaw)	M_a	Added mass matrix
		m_0	Standard deviation

Corresponding author: *Seung Jae Lee*, e-mail: *slee@kmou.ac.kr*

N	Number of time step	$\ddot{x}_i$	Acceleration of Ship, i=1(Surge), i=2(Sway), i=6(Yaw)
S_W	Wetted surface		
T_e	Encounter wave period	Y_d	Desired course for autopilot
U	Ship velocity	β	Drift angle of ship
x_6	Heading angle	δ_s, δ_p	Rudder angles of starboard and port rudders
x_G	Location of center of gravity of ship in x-axis direction force	$\delta_{S,1/3}$	Significant rudder angle on Starboard
		χ	Wave direction
$\dot{x}_6$	Yaw rate of ship	ω	Wave frequency
$\dot{x}_i$	Velocity of Ship, i=1(Surge), i=2(Sway), i=6(Yaw)	ω_e	Encounter wave frequency
		ψ_d	Desired heading angle for autopilot

INTRODUCTION

About eighty percent of the cargo in the world is transported by ships, and thus the position of ship in the global transport industry is dominant in comparison of any other transport means. However, carbon emission by ships accounts for 3.3% of that of the entire world, which is not a negligible ratio. Since individual countries that agreed on the Kyoto Protocol in 1997 should carry out the greenhouse gas reduction that they have promised, international attention is paid to greenhouse gas emission. With respect to ships, the International Maritime Organization (IMO) made the decision in 2012 to introduce a guideline about greenhouse gas reduction for newly built ships. Therefore, from January 2013, newly built ships must satisfy the Energy Efficiency Design Index (EEDI) (IMO, 2012a). In addition, existing ships are recommended to fill the Ship Energy Efficiency Management Plan (SEEMP) and the Energy Efficiency Operational Indicator (EEOI) to strengthen the regulation on the greenhouse gas emission from the ships now in operation. Moreover, beside the IMO regulations, EU is planning to impose bunker levy on ships. Therefore, it is expected that regulations on greenhouse gas emission will be intensified further.

To satisfy EEDI, alternatives such as use of nitrogen oxide reduction catalysis instrument, desulfurization equipment, and high-price low sulfur oil have been suggested, but increase of shipbuilding cost and operating cost is unavoidable when these alternatives are applied. Hence, to develop environment-friendly, green ships as a new paradigm, it is required to develop technologies for reducing carbon emission and energy consumption. With respect to the recently developed energy saving method for ships, Lee et al. (2012) suggested installing a crown duct, which is an energy-saving device, in front of a propeller to control the propeller inflow to increase the propulsion efficiency, and Lamas et al. (2013) suggested a method of reducing NOx by improving operation in an engine and verified the method through numerical analysis. In addition, to reduce gas emission of an actual ship, Kim et al. (2012) proposed an optimal cruising speed to reduce fuel consumption. Study has also been conducted on the improvement of advancing performance by special rudder system. Nagarajan et al. (2008) performed a simulation of identical ships having a normal rudder and a Schilling rudder and verified the advancing performance of ships having a Schilling rudder was higher under strong wind condition. In shipbuilding industry in Korea also, various studies are conducted by individual shipbuilding companies to reduce greenhouse gas emission by performing projects such as Green Dream ECO-Ship by utilizing new renewable energy sources (wind, solar light, etc.) and developing energy-saving devices.

One of the solution to meet EEDI is to lower a ship speed to achieve the required EEDI. To avoid negative effect such as under-powered ships, the 64th Conference of EEDI Marine Environment Protection Committee (MEPC) held in 2012 provided guidelines for the minimum propulsion force to maintain maneuverability under adverse conditions as an EEDI consideration for a new ship. The adverse conditions of sea environment are set by the parameters shown in Table 1 (IMO, 2012b).

Table 1 Adverse mean sea condition for EEDI.

Significant wave height	6.0 *m*
Peak wave period	8.0 to 15.0 *sec.*
Mean wind speed	19.0 *m/s*

Although the conditions shown in Table 1 are adverse conditions, the present study was conducted by considering that ships always face sea environment conditions. In addition, with a given shape of ship and propulsion performance, transporting cargos in a shorter time may help to reduce fuel consumption and gas emission. The purpose of this study was to analyze the effect of controlling rudder in regular waves on the advancing speed of a ship. For this, a three-degrees-of-freedom simulation was performed by using the commercial software program, AQWA. The simulation was reconstructed by adding a subroutine prepared for the calculation of the rudder force and propeller thrust. An autopilot simulation for a ship in regular waves was constructed to compare the ship advancing speed depending on rudder controllers.

Coordinate systems and equation of motion

Only planar motion consisting of three degrees of freedom for surge, sway, and yaw was taken into account in the simulation. The AQWA-NAUT used for the simulation basically allows calculating motion of six degrees of freedom, but the simulation was performed by forcefully fixing heave, roll, and pitch to focus on ship advancing performance depending on rudder controllers. The coordinate systems which is used for describing the position and velocity parameters in the simulation are shown in Fig. 1. The fixed coordinates were denoted as X and Y, and the coordinate axes with a moving ship were defined as x_1 and x_2. The wave incidence angle (χ) was expressed by defining the wave moving from the stern to the bow as 0° when a ship is in an initial position on the origin of the fixed coordinate system. The rotation angle (δ_p, δ_S) of the rudder in parallel with the axis with reference to x_1 is defining 0°.

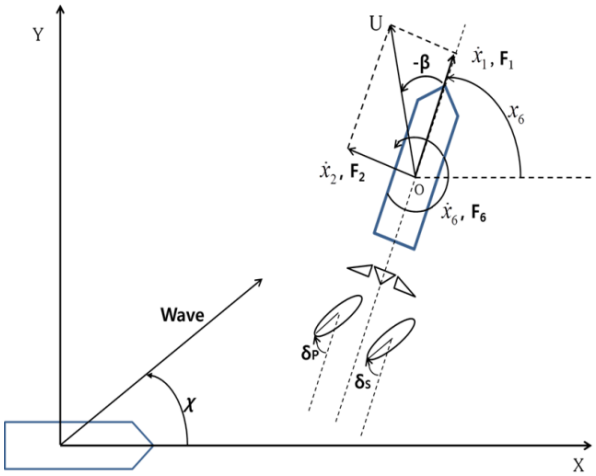

Fig. 1 Coordinate system for simulation.

The ship model used in this study was a 1:78.75 downscaled model of a 315 *m* VLCC. A Vec-twin rudder system, which is one type of single propeller and twin rudder system, was used in the simulation. It is noted that, although most of ships are equipped with single propeller and single rudder, this study simulates single propeller and twin rudder system due to an availability of experimental data of hull, rudder, and propeller coefficients. The difference between two cases may not be large qualitatively. Table 2 shows the principal particulars of the ship model used in the simulation.

Table 2 Principal dimensions of Ship model.

L	4.00 *m*	x_G	0.123 *m*
B	0.667 *m*	S_W	4.049 m^2
d_m	0.24 *m*	D_P	0.1206 *m*
C_b	0.817	A_R / Ld_m	1/71.0
Even keel condition with Mariner type super Vec-twin rudder			

The three-degrees-of-freedom equation of motion used in the simulation is expressed as in Eq. (1). The subscription i represents modes of motion that 1, 2, and 6 refer to surge, sway, and yaw, respectively. It is known that the analysis of motion including roll may provide more accurate results in the simulation considering the effect of waves. However, in the present study, to employ the experimental coefficients of Kang et al. (2008) as the coefficients for the mathematical model for rudders and a propeller, the simulation was constructed without roll motion. The right side of Eq. (1) representing external force is defined as wave exciting force, nonlinear hydrodynamic force, rudder force, and propeller thrust, as shown in Eq. (2).

$$(M_s + M_a)\ddot{x}_i + C\dot{x}_i + K(t) = F_i \tag{1}$$

$$F_i = F_{W,i} + F_{H,i} + F_{R,i} + F_{P,i} \tag{2}$$

The procedure for calculating hydrodynamic load on a ship with AQWA-NAUT was constructed with reference to AQWA User's Manual (Ansys, 2012). Added mass (M_a), damping factor (C), stability coefficient (K), and $F_{W,i}$ which is the sum of Froude-Krylov force and diffraction force, were to be calculated in each time step by AQWA-NAUT. Even though drift force of waves are one of important factors in ship's maneuverability, this study only considers Foude-Krylov force and diffraction force which affects maneuverability at relatively high frequency because verification of relation between rudder controller and ship speed is main target of this study. An additional subroutine was constructed to calculate the remaining external force term in Eq. (2). To apply nonlinear hydrodynamic hull force ($F_{H,i}$) to the simulation, the regression model by Kijima and Nakiri. (2003) was employed. For the resistance coefficient having the greatest effect on the advancing performance, the value from model experiment was included in $F_{H,1}$ term in Eq. (2). The experimental coefficients by Kang et al. (2008) were employed to develop the mathematical models for the propeller thrust and rudder force of the Vec-twin rudder system in the simulation. A subroutine was constructed in order that the nonlinear hydrodynamic force, propeller thrust, and rudder force are calculated in each time step, and the results are substituted in the equation of motion.

Simulation setting

To carry out a simulation with AQWA-NAUT, it should be preceded to obtain Response Amplitude Operators (RAOs) of ship motion according to the wave force. This is because the diffraction force is calculated with diffraction potential calculated in frequency domain according to the information of the wave which locates at the center of a ship, while the Froude-Krylov force is calculated in each time step according to the wetted surface area of a ship depending on the wave. Since the result of ship motion is dependent on the size of mesh used for ship modeling, the convergence of result should be verified depending on the mesh size to improve the accuracy of hydrodynamic calculation. Therefore, the motion RAOs were calculated and compared with seven kinds of ship models in which the number of meshes distributed on ship surface was set to be 410, 550, 880, 1700, 2600, 3100, or 3500.

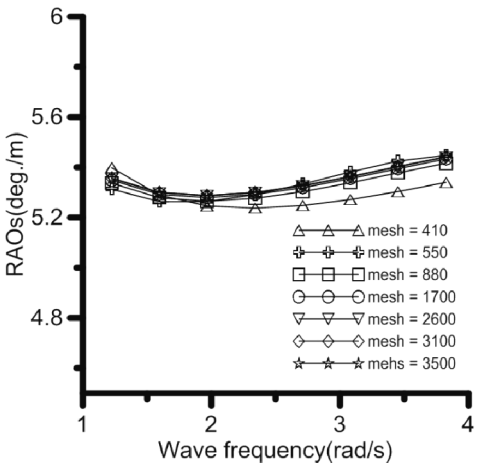

Fig. 2 Magnified Yaw RAOs at 135° wave direction.

Fig. 2 shows the results of yaw RAOs calculation depending on the number of meshes at an incidence wave angle of 135°. The results do not show a significant difference dependent on the number of meshes. However, the results of Case 5 to Case 7 having the mesh number of 2600 or more were the same, indicating that the result was converged. Since an unnecessary increase of the number of meshes causes increased calculation time, the following calculation was performed by using a ship model having 2600 meshes.

Fig. 3 shows the concept of calculation procedures constructing the time domain simulation. The simulation comprises the AQWA-NAUT and additional subroutines. The equation of motion for tracing ship motion was calculated by AQWA-NAUT in each time step. A Dynamic-Link Library (DLL) type subroutine was added to calculate nonlinear hydrodynamic force, rudder force, and propeller thrust, and link them to the equation of motion. After the ship specifications are defined, modeling information, wave conditions, and radiation and diffraction potential forces were put into AQWA-NAUT, AQWA-NAUT calculates the added mass force, wave force decay, and wave exciting force while integrating the equation of motion, and transfers the information of ship heading angle, ship position, and ship velocity to the addition subroutine such as user_force. dll. The nonlinear hydrodynamic force, rudder force, and propeller thrust which are in function of the ship's velocity are calculated simultaneously and the results are transferred to the equation of motion. To perform the advancing simulation under wave conditions, the simulation allows a rudder controller with an autopilot in user_force.dll to control rudder angles and rudder rotational velocity.

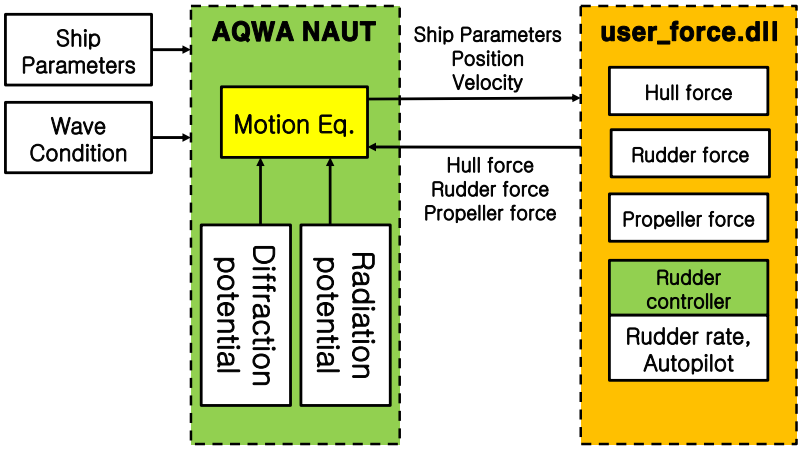

Fig. 3 Concept of time domain simulation.

To compare the variation of ship advancing speed depending on the rudder rotational velocity, seven different rudder rotational velocities were set from 17°/*sec* to 35°/*sec* in 3°/*sec* interval. IMO (2011) provides the standard that the rotation from –35° to 30° should be made within 28 seconds (about 2.32°/*sec* of rudder rotational velocity) in the case of one-propeller and one-rudder ship. Most of ships, except ships including a special rudder system, have a rudder rotational velocity greater than the standard. Among the rudder rotational velocities used for the simulation, the rudder rotational velocities greater than 23°/*sec* satisfy the IMO standard. However the rudder rotational velocity is with reference to the maximum rudder rotational velocity, and there is no constraint in using a rudder rotational velocity which is lower than the IMO standard for autopilot control.

The autopilot controller was employed to construct the ship advancing simulation under wavy condition. The autopilot controller which employed the Proportional Integral Differential (PID) type to control the rudder angle is shown in Eq. (3):

$$\delta_{S,P} = K_P(\psi_d - x_6) - K_D\dot{x}_6 + K_I(Y_d - Y) \tag{3}$$

The controller coefficients of the right side Eq. (3) were set up by repeatedly performing an advancing simulation in a still water condition while varying the controller coefficients. To set up K_P, an advancing simulation was performed to search for the target yaw direction (ψ_d =0°) at the initial yaw direction of 30° as shown in Fig. 4(a). The value which makes the $\sum|x_6|$,

represented by shade in the graph, the minimum was set to be the coefficient. After setting K_P, the calculation was repeated while varying the K_D value to find the K_D value which makes the shaded area the minimum in Fig. 4(b) by the same method used to set up the K_P value. To set up the coefficient of the last term (K_I), the yaw direction 0° and the initial Y coordinate of the ship center was the ship length to perform the simulation. The coefficient which allows for finding the target coordinate ($Y_d = 0$) in 203 seconds (about 30 minutes for an actual ship) was set to be K_I in Fig. 4(c). This was because a too fast return to the original waterway in a case of a deviation from the waterway may cause an excessive yaw angle and yaw rate. It is noted that autopilot coefficients need to be determined under environmental condition of the route including current, wind, and wave drift force. In this study, autopilot coefficients are determined from calm water simulation in order to systematically consider the effect of change of rudder rotational velocity minimizing other factors. Table 3 shows the autopilot coefficients for each rudder rotational velocity obtained by repeated calculations.

Since the simulation was performed based on the ship model scale, it was necessary to scale the ship speed and the wave conditions. The scale ratio of 1:78.75 for the ship size was used to set up the ship speed of 0.806 *m/s* as the initial ship speed corresponding to the actual ship speed of 15 *knots*. The regular wave conditions were set up by referring the adverse wave conditions presented in Table 1 and are shown in Table 4. Table 4 shows the wave amplitude, wave period, and wave direction of the actual ships as well as the ship models used in the simulation.

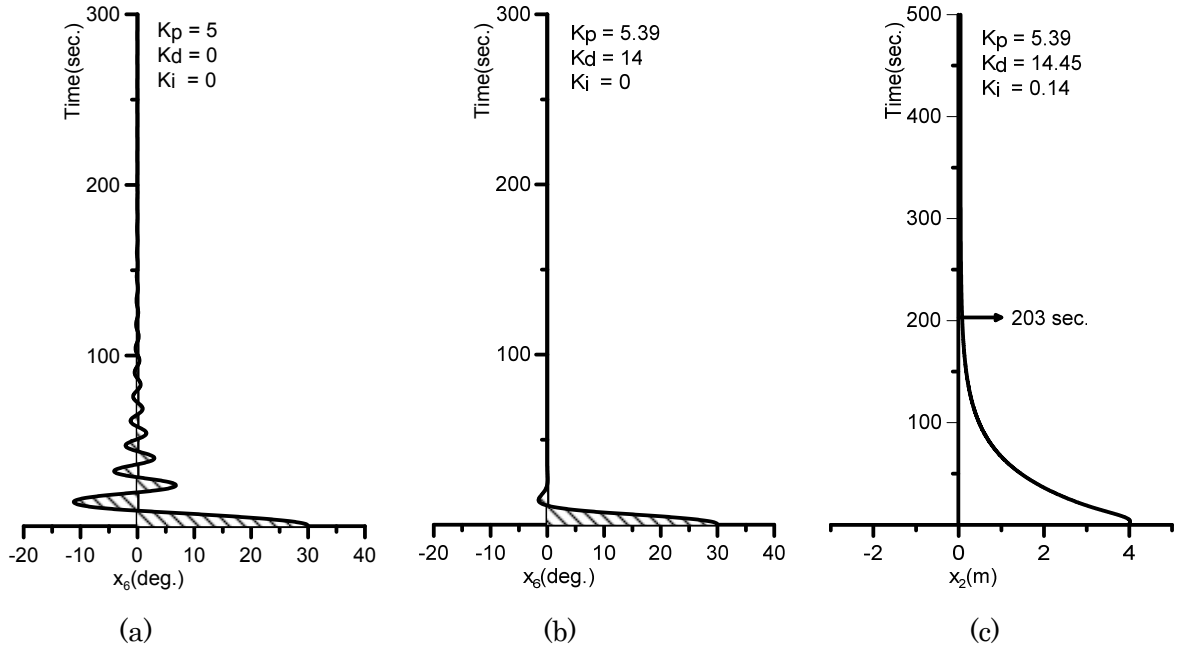

Fig. 4 Example of autopilot setting.

Table 3 Autopilot coefficients for Rudder rotational velocities.

Rudder rotational velocity (*deg./sec*)	K_P	K_D	K_I
17	4.55	13.23	0.112
20	4.75	13.14	0.117
23	5.39	14.45	0.132
26	5.55	14.39	0.137
29	6.14	15.38	0.151
32	6.45	15.9	0.159
35	7.08	16.91	0.174

Table 4 Regular wave conditions for simulations.

Wave amplitude (Ship)	Wave amplitude (Model)	Wave period (Ship)	Wave period (Model)	Wave direction
3 *m*	0.0381 *m*	8.87 *sec.* 11.57 *sec.*	1 *sec.* 1.3 *sec.*	45° 90° 135°

SIMULATIION RESULTS

Fig. 5 shows the yaw RAOs of the ship obtained from AQWA-LINE. The wave frequency corresponding to 1.0 second of the wave period was expressed as a dotted line arrow, and the wave frequency corresponding to 1.3 second of the wave period was expressed as a solid line arrow. The yaw RAOs showed a similar response at the wave directions of 45° and 135°, but the responses at the wave period of 1.3 *sec*. were greater than those at the wave period of 1.0 *sec.* in cases of wave directions 45° and 135°. From this result, it may be predicted that the yaw angle may be greater at the wave period of 1.3 *sec*.

Fig. 6 shows the mean forward speed of the ship during 1000 seconds of autopilot simulation. The horizontal axis is the rudder rotational velocity, while the vertical axis is the mean forward speed. Figs. 6(a) to (c) show the results for the wave directions of 45°, 90°, and 135°, respectively. The wave period of 1.3 *sec*, represented by triangles, showed a lower forward speed than that of the wave period of 1.0 *sec* in all the wave directions. As predicted from the yaw RAOs in Fig. 5, the extensive variation of the yaw angle by the wave might have affected the forward speed. In addition, as the rudder rotational velocity was increased, the forward speed of the ship was decreased, except at the rudder rotational velocity of 17°/sec. It was expected that the forward speed would be increased as the rudder rotational velocity was increased due the enhanced response of the rudder to the wave force, but the tendency was the opposite.

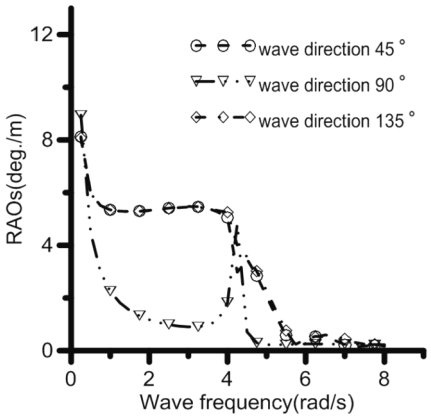

Fig. 5 RAOs of yaw direction.

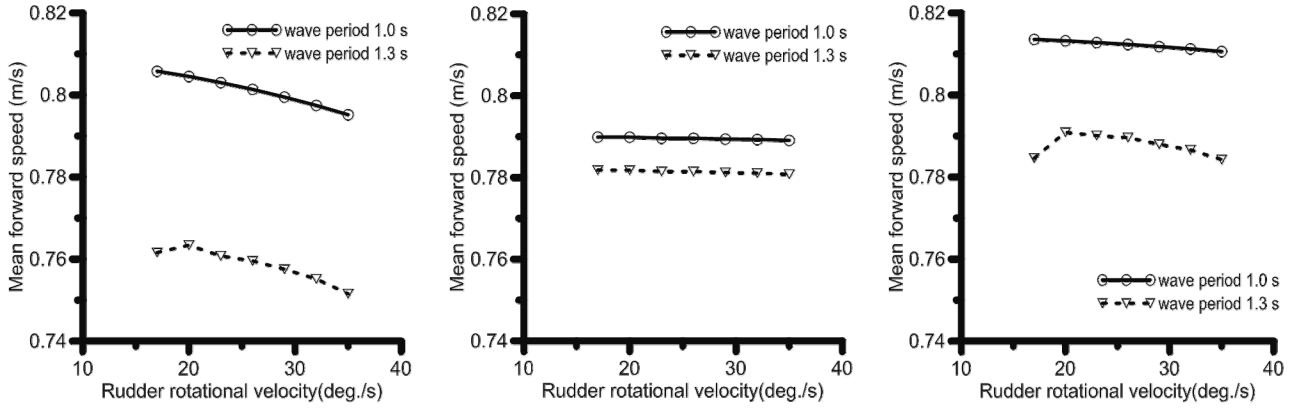

(a) Wave direction 45°. (b) Wave direction 90°. (c) Wave direction 135°.

Fig. 6 Mean forward speed with various rudder rotational velocities.

To analyze the results of the forward speed, the encounter wave period (T_e) depending on the individual wave directions and wave periods was calculated by using Eqs. (4) and (5). The calculated encounter wave periods depending on each wave condition are shown in Table 5.

$$T_e = \frac{2\pi}{\omega_e} \tag{4}$$

$$\omega_e = \omega + \frac{\omega^2 U}{g}\cos(\chi - \beta) \tag{5}$$

Table 5 Period of encounter.

Wave direction period	45°	90°	135°
1.0 *sec.*	1.57 *sec.*	1 *sec.*	0.73 *sec.*
1.3 *sec.*	1.81 *sec.*	1.3 *sec.*	1.02 *sec.*

The encounter wave period, which is the period when the ship center encounters the wave peaks, was from 0.73 *sec.* to 1.81 *sec.*, as shown in Table 5. When the wave force is acting on the ship, the rudder rotates according to the control by autopilot to maintain the heading angle. Due to the periodic characteristic of wave load, the rudder then rotates in the opposite direction of the previous rotation and then rotates again in the direction of the previous rotation. This period should be in between 0.73 *sec.* and 1.81 *sec.* to respond against the wave force effectively.

The significant rudder angle during the simulation was calculated by using Eqs. (6) and (7). The significant rudder angle refers to the mean of the top 1/3 of the rudder angle in the simulation.

$$\delta_{S,1/3} = 4.0\sqrt{m_0} \tag{6}$$

$$m_0 = \frac{1}{N}\sum_{n=1}^{N}(\delta_{S,n} - \delta_S)^2 \tag{7}$$

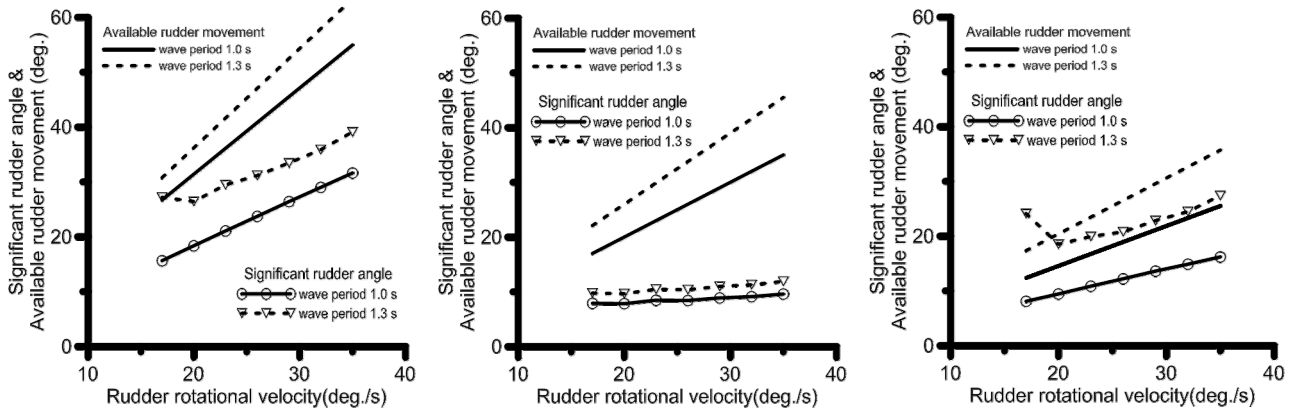

(a) Wave direction 45°. (b) Wave direction 90°. (c) Wave direction 135°.

Fig. 7 Significant rudder angle and available rudder movement.

Fig. 7 shows the significant rudder angle in the simulation with each rudder rotational velocity and the available rudder movement which means maximum rudder angle at rudder rotational velocity during each wave period in Table 5. In the case 135° of wave direction and 17°/*sec* of rudder rotational velocity, the available rudder movement within the encounter wave

period was smaller than the significant rudder angle. This indicates that the heading angle may not be effectively controlled by using the rudder. Therefore, the ship speed was decreased under the same condition shown in Fig. 6. In the case 45° of wave direction and 17°/*sec* of rudder rotational velocity, the available rudder movement was greater than the significant rudder angle, but the difference was small. Since the significant angle that represents the average of top 1/3 of the rudder angle, the rudder angle which is greater than the significant rudder angle exists during the simulation. In this case, the control with the available rudder movement could not be performed effectively, and thus the forward speed might have been decreased. It was verified that there is not a case, except the cases with 17°/*sec* of rudder rotational velocity, which the available rudder rotation within the encounter wave period is lesser than the significant rudder angle.

Fig. 8 shows the mean rudder force in the x-direction of ship-fixed coordinate for 1000 seconds of the simulatoin. The horizontal axis represents the rudder rotational velocity, while the vertical direction represents the mean rudder force in the x-direction. Figs. 8(a) to (c) show the results for the wave directions of 45°, 90°, and 135°, respectively. The tendency of the mean rudder force in the x-direction was similar to that of the significant rudder angle in Fig. 7. This indicates that the heading angle is controlled by using a large rudder angle when the rudder rotational velocity is higher, resulting in an increased rudder force in the x-direction. Since the increased rudder force in the x-direction acted as a greater drag force to the ship, and thereby the ship speed is decreased. It can be also understand that the forward speed at the wave period of 1.3 *sec.* was lower than that at the wave period of 1.0 *sec.*, because the usage of a greater rudder angle caused a greater drag on the ship.

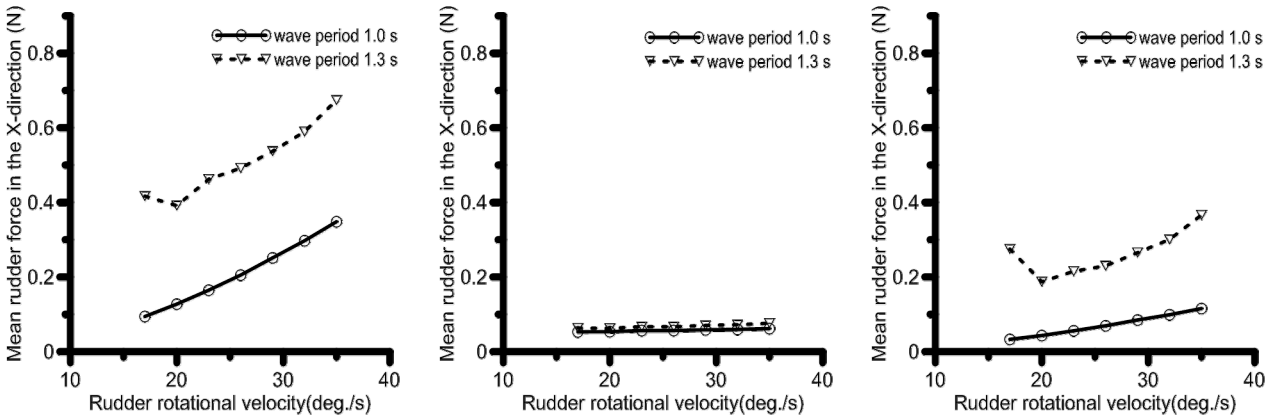

(a) Wave direction 45°. (b) Wave direction 90°. (c) Wave direction 135°.

Fig. 8 Mean Rudder force in the X-direction.

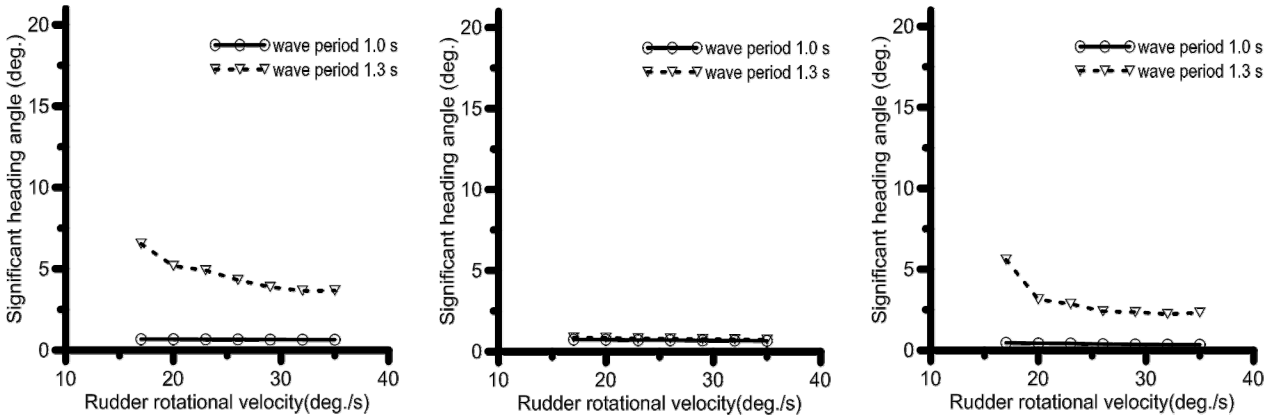

(a) Wave direction 45°. (b) Wave direction 90°. (c) Wave direction 135°.

Fig. 9 Significant heading angle.

Fig. 9 shows the significant heading angle in the simulation. The significant heading angle was calculated by the same method as the calculation of the significant rudder angle. Figs. 9(a) to (c) show the results for the wave directions of 45°, 90°, and 135°, respectively. The larger heading angle fluctuation was found at the wave directions of 45° and 135° at the wave period

of 1.3 *sec.* This also explains the reason why the ship forward speed was lower at the wave period of 1.3 *sec.* than at that of 1.0 *sec.* At the wave direction of 90°, the heading angle fluctuation was not much different between the wave periods of 1.0 *sec.* and 1.3 *sec.*, indicating that the forward speed was mostly affected by the drag on the rudder which is shown in Fig. 8. In addition, although the heading angle fluctuation was not greatly dependent on the rudder rotational velocity at the wave period of 1.0 *sec*, the difference in the forward speed shown in Fig. 6 might have been also caused by the rudder force in the x-direction shown in Fig. 8. Summarizing these results, it may be concluded that decreasing the rudder rotational velocity helps to increase the forward speed of the ship, if the heading angle can be controlled by applying the lower rudder rotational velocity.

Determining the autopilot coefficients according to the individual rudder rotational velocity requires a lot of effort such as Fig. 4. Therefore, the autopilot coefficients which are obtained from the case with the rudder rotational velocity of 23°/*sec* were used to perform the simulations with all others rudder rotational velocities respectively, and the results are shown in Fig. 10. At the wave period of 1.3 *sec.*, the forward speed was the similar or decreased while the rudder rotational velocity decreases. However, at the wave period of 1.0 *sec.*, the forward speeds were increased in the simulations with the rudder rotational velocity is 17°/*sec* and 20°/*sec* at the wave directions of 45° and 135°. The tendency of results is similar with the simulation with their own autopilot coefficients. The forward speeds were decreased at the wave period of 1.3 *sec.*, the wave angles of 45° and 135°, and the rudder rotational velocities of 17°/*sec* and 20°/*sec*, since the heading angle was not effectively controlled by autopilot controller. However, at the wave period of 1.0 *sec.* which enables to control the heading angle by using the lower rudder rotational velocity, therefore the ship forward speed was increased. This result indicates that the forward speed may be improved by decreasing the rudder rotational velocity even without re-establishing the autopilot coefficients, if the heading angle can be controlled. Although the simulation was performed under the regular wave conditions, it was verified that decreasing the rudder rotational velocity may be one of the methods of decreasing the reduction of forward speed due to the wave.

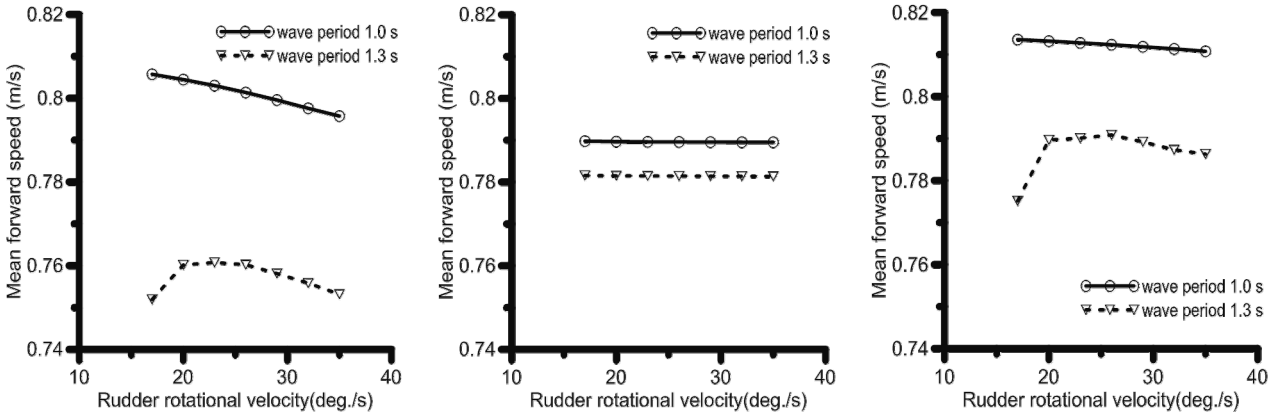

(a) Wave direction 45°. (b) Wave direction 90°. (c) Wave direction 135°.

Fig. 10 Mean forward speed with autopilot coefficient for 23°/*sec* rudder rotational velocity.

CONCLUSIONS

In this study, the forward speed of a ship under wavy condition depending on rudder controllers was investigated by performing a time domain simulation. A commercial simulation tool (AQWA) was used to construct the simulation with three degrees of freedom. While the wave exciting force acting on the ship in the simulation was obtained by AQWA, an additional subroutine calculates the nonlinear hydrodynamic force, rudder force, and propeller thrust in connection with the simulation. Regular waves were used as the disturbance to the ship motion in the simulation, and the effect depending on the variation of the rudder rotational velocity and the autopilot coefficient to ship's forward speed was verified with the results of the autopilot simulation. The conclusions of this study are summarized as follows:

1) The simulation of a ship with three degrees of freedom under regular waves was constructed by using a commercial software program (AQWA) and an additional subroutine which is calculating nonlinear hydrodynamic force, rudder force, and propeller thrust.

2) In the autopilot simulation, the effect of rudder rotational velocity on the forward speed was analyzed with the significant rudder angle, significant heading angle, and drag on rudder.
3) It was verified that ship's forward speed under the regular waves may be improved by decreasing the rudder rotational velocity even without re-establishing the autopilot coefficients, if the heading angle can be controlled with a lower rudder rotational velocity.

ACKNOWLEDGEMENTS

This work was supported by the BK21 PLUS Project and the Research and Business Development Project (2013BS015).

REFERENCES

Ansys, 2012. *AQWA™-LINE manual release 14.5*. Canonsburg: Ansys.

IMO, 2011. *Consideration of IACS unified interpretations and amendments to the ESP code, sub-committee on ship design and equipment 56th session agenda item 13*. London: IMO.

IMO, 2012a. *Guidelines on the method of calculation of the attained energy efficiency design index for new ships, Resolution MEPC, 212(63)*. London: IMO.

IMO, 2012b. *Air pollution and energy efficiency. marine environment protection committee 64th sesson agenda item 4, MEPC 64/4/13*. London: IMO.

Kang, D.H., Nagarajan, V., Hasegawa, K. and Sano, M., 2008. Mathematical model of single-propeller twin-rudder ship. *Journal of Marine Science and Technology*, 13(3), pp.207 -222.

Kijima, K. and Nakiri, Y., 2003. On the practical prediction method for ship manoeuvring characteristics. *Proceedings of International conference on marine Simulation and Ship Maneuverability*, Kanazawa, 25-28 August 2003, pp.RC-6-1-RC-6-10.

Kim, S.K., Lee, Y.S., Kong, G.Y., Kim, J.P. and Jung C.H., 2012. A Study on the ship's speed for reducing the fuel oil consumption in actual ships. *Journal of the Korean Society of Marine Environment & Safety*, 18(1), pp.41-47.

Lamas, M.I., Rodrigusz, C.G., Rodrigues, J.D. and Telmo, J., 2013. Internal modifications to reduce pollutant emissions from marine engines. A numerical approach. *International Journal of Naval Architecture and Ocean Engineering*, 5(4), pp.493-501.

Lee, K.J., An, J.S. and Yang, S.H., 2012. A study on the development of energy-saving device "Crown Duct". *Journal of Ocean Engineering and Technology*, 26(5), pp.1-4.

Nagarajan, V., Kang, D., Hasegawa, K. and Nabeshima, K., 2008. Comparison of the mariner schilling rudder and the mariner rudder for VLCCs in strong winds. *Journal of Marine Science and Technology*, 13, pp.24-39.